PROCEEDINGS OF SCIENCE

Studying electroweak few-body observables in chiral effective field theory

Alex Gnech[a,b,*]

[a] *Department of Physics, Old Dominion University, Norfolk, VA 23529, USA*
[b] *Theory Center, Jefferson Lab, Newport News, VA 23610, USA*

E-mail: agnech@odu.edu

The use of nuclei to study electroweak probes is becoming increasingly relevant experimentally. The success of dark matter and neutrino experiments strongly depends on the ability to control nuclear effects in order to extract the fundamental parameters associated with external probes. Therefore, reliable theoretical calculations of nuclear structure and reactions, with well-controlled errors, are crucial for the success of experimental efforts. Currently, chiral effective field theory (χEFT) coupled with *ab-initio* methods represents one of the best approaches that fulfills these requirements. To use this approach as a tool for studying fundamental physics, it is essential to validate it against experimental data for which the calculations are well under control, such as the elastic scattering of electrons on nuclei. In this proceeding, I will present recent developments in the fitting of electromagnetic currents derived using χEFT and the calculation of electromagnetic form factors of light nuclei. The results of these calculations demonstrate the strength of the theory in describing the interaction of nuclei with electromagnetic probes over a broad range of momentum transfers and highlight the robustness of χEFT for analyzing future experimental data aimed at extracting fundamental parameters.

The 11th International Workshop on Chiral Dynamics (CD2024)
26-30 August 2024
Ruhr University Bochum, Germany

*Speaker

 ISSN 1824-8039 . Published by SISSA Medialab.

PoS(CD2024)009

1. Introduction

Since the seminal work by Weinberg [1, 2], chiral effective field theory (χEFT) has been successfully used to construct nuclear interactions [3, 4] that are directly connected to the QCD Lagrangian. χEFT is based on a separation of scales, where the low-energy effective degrees of freedom are treated dynamically, while all remaining degrees of freedom above the breaking scale energy of the theory ($\Lambda_\chi = 1$ GeV) are integrated out. The low-energy effective Lagrangian is constructed using nucleons, pions, and deltas as degrees of freedom. The interactions among these dynamical degrees of freedom are constrained using the approximate chiral symmetry that appears at the level of the Quantum Chromodynamics (QCD) Lagrangian, along with Lorentz invariance and the conservation (or explicit breaking) of discrete symmetries. The dynamics of the excluded degrees of freedom are encapsulated in the so-called Low Energy Constants (LECs), which multiply the χEFT terms in the Lagrangian and are typically determined by fitting low-energy nuclear data.

The nuclear interactions derived using χEFT offer several advantages: (i) they are directly connected to QCD; (ii) their operators can be organized as a power expansion in Q/Λ_χ, where Q is the typical momentum exchanged in the nuclear process; (iii) the theoretical error can be estimated from the truncation of the power expansion [3, 5]. These reasons make χEFT interactions the preferred choice of *ab initio* practitioners for describing the nucleus as a collection of nucleons interacting via two- and three-nucleon forces. Consistent comparisons with available experimental data have repeatedly confirmed the validity of this theoretical approach.

One of the strengths of χEFT is its ability to describe interactions with electroweak probes within a consistent framework. The interaction of nuclei with leptons can be described through nuclear electroweak currents, which can be organized as a power expansion in a similar fashion to nuclear interactions. This approach has been successfully used to predict low-energy electroweak observables, such as electromagnetic moments [6–10] and transitions [11–15], as well as beta decays (see, for example,[16–19]). The use of χEFT beyond the low-energy/low-momentum regime has been primarily explored in the $A = 2 - 3$ systems[6, 20, 21] and only more recently in larger systems [22–24]. Such studies are crucial for testing the predictive power of the theory in kinematic regimes relevant to experiments, including superallowed β-decay [25–27], neutrinoless double-beta decay [28–31], and long-baseline neutrino oscillation experiments [32–38].

This proceeding focuses on presenting the results of recent work [6, 22, 23] by the JLab-Pisa group in collaboration with the Quantum Monte Carlo group at Washington University in St. Louis on the calculation of electromagnetic few-body observables of light nuclei using χEFT interactions and currents. This manuscript is organized as follows. In Section 2, we present the currents used in this work. In Section 3, we discuss the determination of the Low Energy Constants appearing in the electromagnetic currents. In Section 4, we present selected results for the magnetic form factors in few-body nuclei. Finally, in Section 5, we summarize our conclusions and outline future perspectives of this work.

2. Electromagnetic currents in Chiral Effective Field Theory

The nuclear electromagnetic currents and charge up to one loop in χEFT have been derived independently by the JLab-Pisa group [20, 39–41] using time-ordered perturbation theory, and

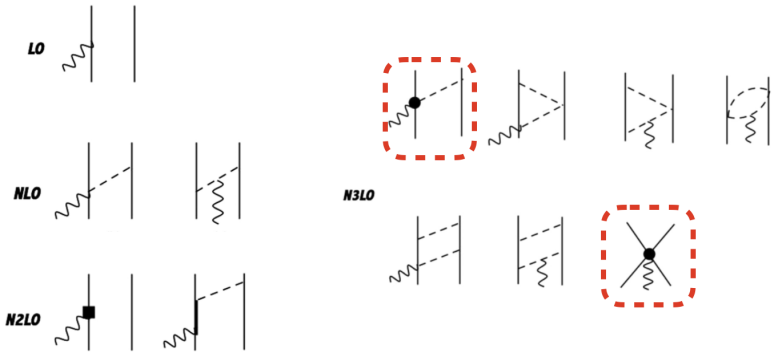

Figure 1: Diagrams appearing in the χEFT expansion of the electromagnetic current up to N3LO in the JLab-Pisa power counting scheme. The red-framed diagrams correspond to those in which unknown LECs appear.

by the Bochum group using the heavy baryon approach [42–44]. In our work, we adopt the formulation derived by the JLab-Pisa group and refer to the notation and power counting established in Refs. [20, 39].

In the JLab-Pisa approach, the diagrams contributing to the electromagnetic current at various orders in the χEFT expansion are shown in Figure 1.

At leading order (LO), the only contribution comes from the single-nucleon current, corresponding to what is known as the impulse approximation. This term appears in the χEFT power counting at order eQ^{-2}. At next-to-leading order (NLO), which in our power counting scheme corresponds to eQ^{-1}, contributions from one-pion exchange diagrams arise.

At next-to-next-to-leading order (N2LO-eQ^{-1}), two additional contributions appear. The first is a relativistic correction to the LO one-body current, while the second arises from the excitation of the Δ-isobar. The latter diagram appears only in versions of χEFT that explicitly include Δ degrees of freedom, as is the case for the Norfolk interactions [45–49], which will be used in the calculation of the observables.

At next-to-next-to-next-to-leading order (N3LO-eQ^{0}), several contributions emerge. The first comes from one-loop two-pion-exchange diagrams, shown in Figure 1. The second consists of contact terms, which are generated by minimal substitution in four-nucleon contact terms involving two gradients of the nucleon fields, as well as by non-minimal couplings to the electromagnetic field. The two operators appearing in the non-minimal coupling terms are associated with two unknown LECs, d_1^S and d_1^V, where S refers to the isoscalar operator and V to the isovector one. The third contribution consists of subleading terms induced by the $\gamma\pi N$ interactions in the one-pion-exchange diagrams. The isovector terms can be related to the $N-\Delta$ transition [39] and introduce two additional unknown LECs, labeled d_2^V and d_3^V. The isoscalar term in the subleading one-pion-exchange contribution is associated with the $\gamma\pi\rho$ current and also has an unknown LEC, d_2^S, which must be determined.

Each operator in the current is associated with the appropriate nucleon isovector/isoscalar electromagnetic form factors, except for the terms related to the Δ and ρ, where the $\gamma N\Delta$ and $\gamma N\rho$ form factors are used. This ensures the proper falloff behavior as the momentum transfer increases in electromagnetic observables. In the JLab-Pisa approach, we use phenomenological form factors

whose parameters are fitted to reproduce experimental data rather than deriving them consistently within chiral perturbation theory [50]. It should be noted that in our power counting, we ignore the fact that the form factors themselves also have a power series expansion in Q.

In the present work, we focus on results obtained using a set of chiral interactions known as the Norfolk family [45–47]. The Norfolk two-body interactions (NV) are local Δ-full interactions derived in χEFT up to N3LO. A long-range (R_L) and a short-range (R_S) cutoff are used to regularize the interaction. Two cutoff pairs are available: $(R_L, R_S) = (1.2\,\text{fm}, 0.8\,\text{fm})$ and $(R_L, R_S) = (1.0\,\text{fm}, 0.7\,\text{fm})$, labeled as model a and model b, respectively. Additionally, model classes I and II correspond to fits of the NN interaction up to 125 MeV and 200 MeV, respectively. In addition to the two-body interaction, a three-body force is included, with its LECs fitted to reproduce the triton binding energy and Gamow-Teller beta decay for each NV model [48].

In this manuscript, we discuss only the results obtained using the NVIIa and NVIIb models. For the results presented here, the currents have been regularized consistently with these two interactions. For a more detailed discussion of the currents, form factors, and regularization used in the calculations presented below, we refer to Ref. [6].

3. Fitting the Low Energy Constants

As with the nucleon-nucleon interaction, the low-energy constants (LECs) appearing in the currents are determined using electromagnetic nuclear data. The historical approach to this determination involves fitting the five LECs to the static magnetic moments of the deuteron, ^{3}He, and ^{3}H [20, 21]. Since only three independent data points are used, this approach requires assuming that the Δ-isobar saturates the LECs d_2^V and d_3^V to reduce the number of free parameters in the fit. However, this method fails to reproduce the magnetic form factors of light nuclei in the momentum transfer region of $q \sim 1-4\,\text{fm}^{-1}$. In particular, it generates a diffraction feature around $\sim 3\,\text{fm}^{-1}$ for ^{3}He, which is displaced from the physical diffraction minimum observed at $\sim 4\,\text{fm}^{-1}$ [20, 21]. An extension of this approach was considered in Ref. [7], where the fit included the magnetic moments of nuclei up to ^{18}F. However, no tests have been performed to assess the predictive power of this fit for magnetic form factors.

In Ref. [6], we introduced a new fitting procedure. In addition to the deuteron, ^{3}H, and ^{3}He magnetic moments, we incorporated data from deuteron-threshold electron-disintegration cross-sections at backward angles (d-threshold). Including these data allows us to fit not only static properties but also dynamical aspects of the currents, specifically their dependence on momentum transfer. This is achieved using the two-body neutron-proton (n-p) system, for which nuclear structure calculations are well under control. Furthermore, since this observable is dominated by the isovector transition, it enables us to constrain the LECs associated with isovector operators without relying on Δ-saturation assumptions.

For a detailed discussion of the fitting procedure, we refer to Ref. [6]. Here, we briefly summarize the results. In Figure 2, we present the computed d-threshold cross-section using the NVIIa model, compared with experimental data [51–55]. The orange dashed line represents the calculation including all diagrams up to N3LO but excluding those associated with the five LECs.

As seen in Figure 2, a diffraction region appears around $Q^2 \sim 10 - 15$ fm^{-2}, which is absent in the experimental data. This discrepancy primarily originates from the transition between the $^3S_1 - ^3D_1$ and $^1S_0$ states in the scattering process. However, contributions from higher partial waves beyond $^1S_0$ help to mitigate this effect. The blue dashed line represents the contribution from the fitted isovector current terms, which have the appropriate operator structure to correct the diffraction region and simultaneously suppress the high-energy tail in the d-threshold cross-section produced by the other diagrams. The final result, given by the black curve, exhibits excellent agreement with the experimental data. The yellow band represents the uncertainty associated with the fit.

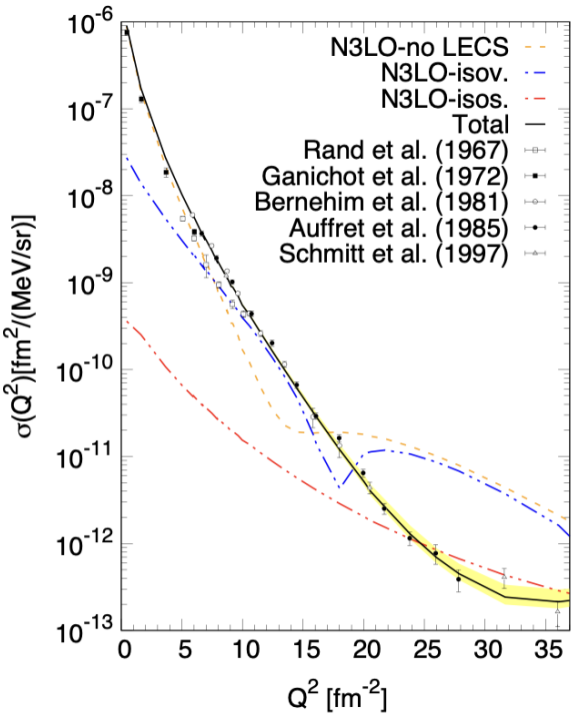

Figure 2: Deuteron-threshold electron-disintegration cross-sections at backward angles. The orange dashed line represents the N3LO calculation without the fitted terms. The blue (red) dot-dashed line represents the contribution from the fitted isovector (isoscalar) terms. The full calculation is given by the black curve, with the yellow band indicating the fit uncertainties. Black circles represent experimental data [51–55].

It is worth noting that the operators corresponding to the isoscalar LECs d_1^S and d_2^S have minimal impact on this observable, as shown by the red dashed line in Figure 2. Instead, these LECs are primarily constrained by the deuteron's magnetic moment. Moreover, including d-threshold data in the fit has a negligible impact on the calculation of the magnetic moments of the three-nucleon systems. Indeed, our fitting procedure reproduces the experimental magnetic moments with good accuracy (see Ref. [6] for a detailed discussion). Similar results have been obtained for all other Norfolk interactions used, as shown in Ref. [6].

4. Prediction of electromagnetic observables in few-body nuclei

The fitted currents have been used to compute the magnetic form factors of light nuclei. In this section, we analyze in detail the magnetic form factor of the trinucleon system [6] using the Hyperspherical Harmonic method [56] and briefly present results for the magnetic form factors of $A = 6 - 10$ nuclei [22, 23], obtained using the Variational Monte Carlo (VMC) method [57] in collaboration with the Quantum Monte Carlo group in St. Louis.

In Figure 3, we present the calculation of the magnetic form factor of ^{3}He using the NVIIa nuclear interaction, compared to experimental data from Ref. [58]. We follow the same color scheme as in Figure 2. The orange dashed line represents the contribution from all diagrams except the fitted ones. These contributions produce a diffraction minimum at a significantly lower momentum

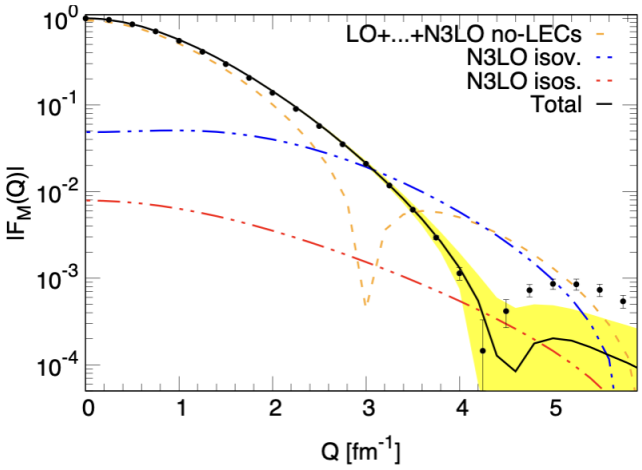

Figure 3: Magnetic form factor of ^{3}He. The line types and colors follow the same convention as in Figure 4. The black circles represent experimental data from Ref. [58].

transfer than the physical one, consistent with previous findings [20, 21]. The fitted isovector terms (blue dashed line) correct this discrepancy by shifting the diffraction minimum to align with experimental data. Additionally, their interference with other diagrams generates a new diffraction region in excellent agreement with the physical one. Notice that the position of the new diffraction region depends on the fine tuning of the isovector LECs. It is important to note that, apart from the normalization of the magnetic form factor (i.e., the magnetic moment), the momentum-transfer dependence is a pure prediction of our theoretical framework. Similar qualitative results have been obtained for ^{3}H and for all other interactions studied in Ref. [6].

The success of this fitting procedure in describing the magnetic form factor at high momentum transfer can be understood through the np-dominance mechanism. Short-range correlation experiments have shown that nucleons inside nuclei tend to form correlated pairs [59], with the most probable configurations being neutron-proton (np) pairs in relative $^1S_0$ or $^3S_1$ states. This naturally leads to the dominance of isovector two-body current transitions. Moreover, since the np $^1S_0$ and $^3S_1$ wavefunctions inside a nucleus are universal (up to a scaling factor) [60], the corresponding isovector transition matrix elements also exhibit universality. Consequently, knowledge of these matrix elements in the d-threshold process allows us to predict their contributions to magnetic form factors and vice versa.

Motivated by these findings, we extended our analysis to heavier nuclei. By combining the VMC method [57] with the newly fitted currents, we computed the magnetic form factors of several nuclei in the mass range $A = 6 - 10$. In this proceeding, we focus on ^{6}Li, ^{7}Li, ^{9}Be, and ^{10}B, for which experimental data are available[1]. Figure 4 presents our results compared to experimental data. In the case of ^{6}Li, the only contribution comes from the $M1$ multipole. For the other nuclei, the diffraction minimum observed in the $M1$ multipole is filled by the $M3$ multipole, leading to the emergence of a second peak in the magnetic form factor. For ^{10}B, an additional contribution from

[1]The full list of experimental data references is provided in Refs. [22, 23]. A digitalized version of the data can be shared by the author upon request.

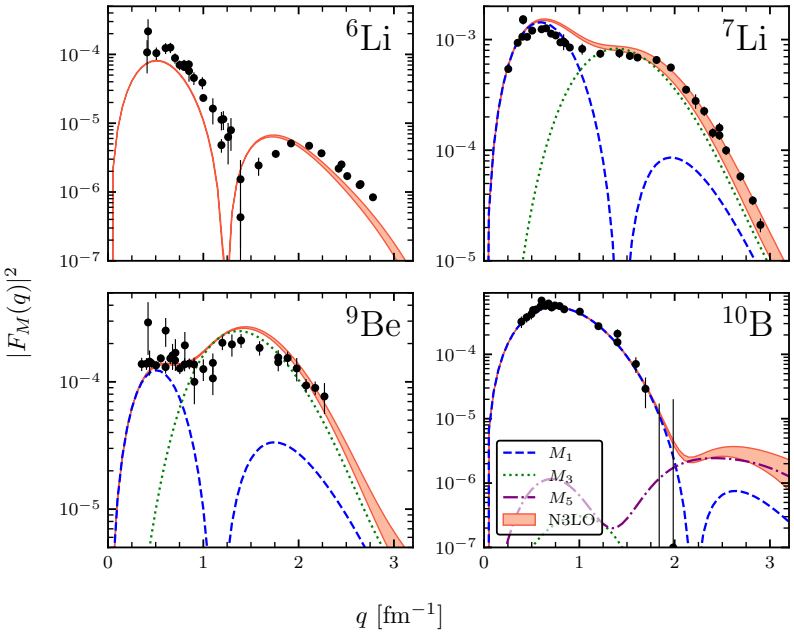

Figure 4: Magnetic form factors of ^{6}Li, ^{7}Li, ^{9}Be, and ^{10}B computed using the NVIIb nuclear interaction. The red band represents the full calculation, with its width indicating uncertainties due to truncation of the nuclear current expansion (following Ref. [3]). The blue-dashed, green-dotted, and purple dash-dotted lines correspond to the contributions of the $M1$, $M3$, and $M5$ multipoles, respectively. Black dots indicate experimental data (see footnote for details).

the $M5$ multipole generates a secondary peak at higher momentum transfer. Notably, this is the first theoretical prediction of this secondary peak, which was only hypothesized in Ref. [61].

Notice that the calculations are able to reproduce the exact magnitude of the data without any renormalization even if some discrepancy remains. For ^{6}Li we are able to reproduce the two peaks even if, for all the interactions considered, the diffraction minimum appears at slightly lower momentum transfer than in experiment, and the second peak is somewhat overestimated. This happens for all the nuclear models used in our work [23]. We think that this is mainly due to a deficiency in the VMC wave function. For ^{7}Li our calculation correctly describes the high-momentum tail when N3LO corrections are included but slightly overestimates the first peak—similar to findings in phenomenological models [61]. In the case of ^{9}Be the low-momentum plateau is well captured due to two-body current contributions, but the second peak is overestimated, indicating a need for fine-tuning between nuclear structure and two-body currents. Further *ab-initio* studies are encouraged to clarify this interplay. Finally for ^{10}B the situation is simpler since the magnetic form factor receives only contribution from the isoscalar terms of the currents and the description of the data is optimal.

In Refs. [22, 23], we also predicted the magnetic form factors for nuclei without experimental data. Specifically, we examined mirror systems: ^{9}Li-^{9}C, ^{7}Li-^{7}Be, and ^{9}Be-^{9}B. For all cases, we observe an enhancement of the $M1$ peak in neutron-rich systems and its suppression in proton-rich counterparts relative to the $M3$ multipole. This pattern arises from constructive (destructive) interference between spin and orbital components in the $M1$ multipole when the dominant unpaired

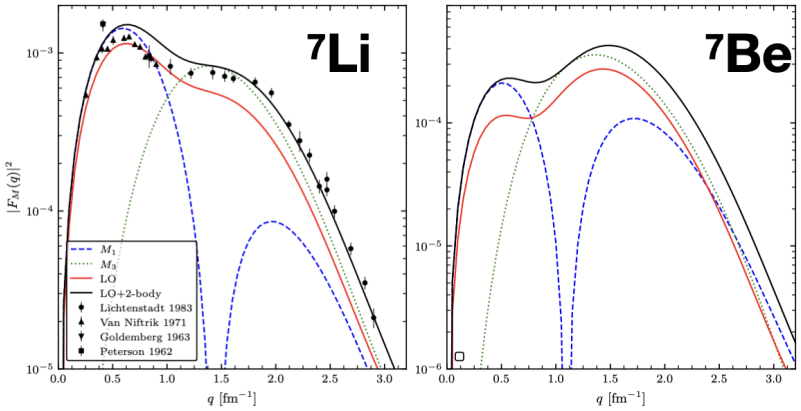

Figure 5: Magnetic form factors of the mirror nuclei ^{7}Li and ^{7}Be. The black (red) solid line represents the full calculation at N3LO (LO). The blue-dashed and green-dotted lines show the $M1$ and $M3$ multipole contributions at N3LO. Black circles represent experimental data for ^{7}Li. Note the enhancement (suppression) of the $M1$ peak relative to $M3$ in ^{7}Li (^{7}Be).

nucleon is a neutron (proton). To our knowledge, this effect has not been previously observed in theoretical calculations, and no experimental data exist for mirror nuclear pairs. We hope future experiments will confirm our predictions.

5. Conclusion and future prospective

In this work, we have demonstrated that electromagnetic currents derived in χEFT can successfully describe the magnetic form factors of light nuclei in the momentum transfer range $q \sim 0-3.5$ fm^{-1}. We fitted the five low-energy constants (LECs) appearing in the N3LO currents to the magnetic moments of the deuteron, ^{3}H, and ^{3}He, as well as to the threshold deuteron electrodisintegration at a backward angle. The inclusion of this last dataset allows us to describe the magnetic form factor at high momentum transfer, providing strong evidence that χEFT has the correct operator structure to do so. It is important to note that in our calculations, we used phenomenological nucleon form factors rather than ones consistently derived from χEFT. Our results for magnetic form factors beyond the $A = 3$ system show excellent agreement with available experimental data. Additionally, we observed, for the first time, the inversion of the relative strengths of the $M1$ and $M3$ multipoles in p-shell mirror systems. Notably, the Quantum Monte Carlo results presented here and in Refs. [22, 23] constitute the first *ab initio* calculations of the magnetic form factors for light p-shell nuclei beyond $A = 6$. We hope this work will encourage other groups to perform similar calculations and inspire experimentalists to obtain higher-precision measurements for a broader range of nuclei. Such improvements would provide better constraints on the theoretical description of electromagnetic currents, which is crucial for future neutrino experiments.

6. Acknowledgment

The work of A.G. is supported by the U.S. Department of Energy through the Nuclear Theory for New Physics Topical Collaboration, under contract DE-SC0023663. A.G. acknowledges also

the support of Jefferson Lab supported by the U.S. Department of Energy under contract DE-AC05-06OR23177.

References

[1] Steven Weinberg. Nuclear forces from chiral Lagrangians. *Phys. Lett.*, B251:288–292, 1990.

[2] Steven Weinberg. Effective chiral Lagrangians for nucleon - pion interactions and nuclear forces. *Nucl. Phys.*, B363:3–18, 1991.

[3] E. Epelbaum, H. Krebs, and Ulf-G. Meißner. Improved chiral nucleon-nucleon potential up to next-to-next-to-next-to-leading order. *Eur. Phys. J. A*, 51:53, 2015.

[4] Maria Piarulli, Jason Bub, and Ingo Tews. *Local Two- and Three-Nucleon Interactions Within Chiral Effective Field Theory*, pages 1–33. 2022.

[5] J. A. Melendez, R. J. Furnstahl, D. R. Phillips, M. T. Pratola, and S. Wesolowski. Quantifying Correlated Truncation Errors in Effective Field Theory. *Phys. Rev. C*, 100(4):044001, 2019.

[6] Alex Gnech and Rocco Schiavilla. Magnetic structure of few-nucleon systems at high momentum transfers in a chiral effective field theory approach. *Phys. Rev. C*, 106(4):044001, 2022.

[7] J. D. Martin, S. J. Novario, D. Lonardoni, J. Carlson, S. Gandolfi, and I. Tews. Auxiliary field diffusion Monte Carlo calculations of magnetic moments of light nuclei with chiral EFT interactions. 1 2023.

[8] Soham Pal, Shiplu Sarker, Patrick J. Fasano, Pieter Maris, James P. Vary, and Mark A. Caprio. Magnetic moments of $A = 3$ nuclei with chiral effective field theory operators. 4 2023.

[9] T. Miyagi, X. Cao, R. Seutin, S. Bacca, R. F. Garcia Ruiz, K. Hebeler, J. D. Holt, and A. Schwenk. Impact of Two-Body Currents on Magnetic Dipole Moments of Nuclei. *Phys. Rev. Lett.*, 132(23):232503, 2024.

[10] S. Lechner et al. Electromagnetic moments of the antimony isotopes ^{112133}Sb. *Phys. Lett. B*, 847:138278, 2023.

[11] S. Pastore, Steven C. Pieper, R. Schiavilla, and R. B. Wiringa. Quantum Monte Carlo calculations of electromagnetic moments and transitions in A $\leq$ 9 nuclei with meson-exchange currents derived from chiral effective field theory. *Phys. Rev.*, C87(3):035503, 2013.

[12] S. Pastore, R. B. Wiringa, Steven C. Pieper, and R. Schiavilla. Quantum Monte Carlo calculations of electromagnetic transitions in ^{8}Be with meson-exchange currents derived from chiral effective field theory. *Phys. Rev.*, C90(2):024321, 2014.

[13] N. M. Parzuchowski, S. R. Stroberg, P. Navrátil, H. Hergert, and S. K. Bogner. Ab initio electromagnetic observables with the in-medium similarity renormalization group. *Phys. Rev. C*, 96(3):034324, 2017.

[14] S. R. Stroberg, J. Henderson, G. Hackman, P. Ruotsalainen, G. Hagen, and J. D. Holt. Systematics of E2 strength in the sd shell with the valence-space in-medium similarity renormalization group. *Phys. Rev. C*, 105(3):034333, 2022.

[15] Anna E. McCoy, Mark A. Caprio, Pieter Maris, and Patrick J. Fasano. Intruder band mixing in an ab initio description of 12Be. 2 2024.

[16] Garrett B. King, Alessandro Baroni, Vincenzo Cirigliano, Stefano Gandolfi, Leendert Hayen, Emanuele Mereghetti, Saori Pastore, and Maria Piarulli. Ab initio calculation of the β-decay spectrum of He6. *Phys. Rev. C*, 107(1):015503, 2023.

[17] G. B. King, S. Pastore, M. Piarulli, and R. Schiavilla. Partial muon capture rates in A=3 and A=6 nuclei with chiral effective field theory. *Phys. Rev. C*, 105(4):L042501, 2022.

[18] G. B. King, L. Andreoli, S. Pastore, M. Piarulli, R. Schiavilla, R. B. Wiringa, J. Carlson, and S. Gandolfi. Chiral effective field theory calculations of weak transitions in light nuclei. *Phys. Rev. C*, 102:025501, Aug 2020.

[19] Alex Gnech, Laura Elisa Marcucci, and Michele Viviani. Bayesian analysis of muon capture on the deuteron in chiral effective field theory. *Phys. Rev. C*, 109(3):035502, 2024.

[20] M. Piarulli, L. Girlanda, L. E. Marcucci, S. Pastore, R. Schiavilla, and M. Viviani. Electromagnetic structure of A = 2 and 3 nuclei in chiral effective field theory. *Phys. Rev.*, C87(1):014006, 2013.

[21] R. Schiavilla, A. Baroni, S. Pastore, M. Piarulli, L. Girlanda, A. Kievsky, A. Lovato, L. E. Marcucci, Steven C. Pieper, M. Viviani, and R. B. Wiringa. Local chiral interactions and magnetic structure of few-nucleon systems. *Phys. Rev. C*, 99:034005, Mar 2019.

[22] G. Chambers-Wall, A. Gnech, G. B. King, S. Pastore, M. Piarulli, R. Schiavilla, and R. B. Wiringa. Quantum Monte Carlo Calculations of Magnetic Form Factors in Light Nuclei. *Phys. Rev. Lett.*, 133(21):212501, 2024.

[23] G. Chambers-Wall, A. Gnech, G. B. King, S. Pastore, M. Piarulli, R. Schiavilla, and R. B. Wiringa. Magnetic structure of A$\leq$10 nuclei using the Norfolk nuclear models with quantum Monte Carlo methods. *Phys. Rev. C*, 110(5):054316, 2024.

[24] G. B. King, G. Chambers-Wall, A. Gnech, S. Pastore, M. Piarulli, and R. B. Wiringa. Longitudinal form factors of A$\leq$10 nuclei in a chiral effective field theory approach. *Phys. Rev. C*, 110(5):054325, 2024.

[25] Chien-Yeah Seng and Mikhail Gorchtein. Dispersive formalism for the nuclear structure correction δNS to the β decay rate. *Phys. Rev. C*, 107(3):035503, 2023.

[26] Vincenzo Cirigliano, Wouter Dekens, Jordy de Vries, Stefano Gandolfi, Martin Hoferichter, and Emanuele Mereghetti. Radiative corrections to superallowed β decays in effective field theory. 5 2024.

[27] Michael Gennari, Mehdi Drissi, Mikhail Gorchtein, Petr Navratil, and Chien-Yeah Seng. An *ab initio* recipe for taming nuclear-structure dependence of V_{ud}: the $^{10}\mathrm{C} \to {}^{10}\mathrm{B}$ superallowed transition. 5 2024.

[28] Jonathan Engel and Javier Menéndez. Status and Future of Nuclear Matrix Elements for Neutrinoless Double-Beta Decay: A Review. *Rept. Prog. Phys.*, 80(4):046301, 2017.

[29] Matteo Agostini, Giovanni Benato, Jason A. Detwiler, Javier Menéndez, and Francesco Vissani. Toward the discovery of matter creation with neutrinoless $\beta\beta$ decay. *Rev. Mod. Phys.*, 95(2):025002, 2023.

[30] S. Pastore, J. Carlson, V. Cirigliano, W. Dekens, E. Mereghetti, and R. B. Wiringa. Neutrinoless double-β decay matrix elements in light nuclei. *Phys. Rev.*, C97(1):014606, 2018.

[31] V. Cirigliano, W. Dekens, J. De Vries, M. L. Graesser, E. Mereghetti, S. Pastore, M. Piarulli, U. Van Kolck, and R. B. Wiringa. A renormalized approach to neutrinoless double-beta decay. *Phys. Rev.*, C100(5):055504, 2019.

[32] Ko Abe, R Akutsu, A Ali, C Alt, C Andreopoulos, L Anthony, M Antonova, S Aoki, A Ariga, Y Asada, et al. Constraint on the matter-antimatter symmetry-violating phase in neutrino oscillations. *arXiv preprint arXiv:1910.03887*, 2019.

[33] M. A. Acero et al. First Measurement of Neutrino Oscillation Parameters using Neutrinos and Antineutrinos by NOvA. *Phys. Rev. Lett.*, 123(15):151803, 2019.

[34] R Acciarri, C Adams, R An, A Aparicio, S Aponte, J Asaadi, M Auger, N Ayoub, L Bagby, B Baller, et al. Design and construction of the microboone detector. *Journal of Instrumentation*, 12(02):P02017, 2017.

[35] L Aliaga, L Bagby, B Baldin, A Baumbaugh, A Bodek, R Bradford, WK Brooks, D Boehnlein, S Boyd, H Budd, et al. Design, calibration, and performance of the minerva detector. *Nuclear Instruments and Methods in Physics Research Section A: Accelerators, Spectrometers, Detectors and Associated Equipment*, 743:130–159, 2014.

[36] Seon-Hee Seo. Physics potentials of the hyper-kamiokande second detector in korea. *arXiv preprint arXiv:1811.06682*, 2018.

[37] Babak Abi, R Acciarri, Mario A Acero, G Adamov, D Adams, M Adinolfi, Z Ahmad, J Ahmed, T Alion, S Alonso Monsalve, et al. Deep underground neutrino experiment (dune), far detector technical design report, volume ii dune physics. *arXiv preprint arXiv:2002.03005*, 2020.

[38] L. Alvarez Ruso et al. Theoretical tools for neutrino scattering: interplay between lattice QCD, EFTs, nuclear physics, phenomenology, and neutrino event generators. 3 2022.

[39] S. Pastore, R. Schiavilla, and J. L. Goity. Electromagnetic two-body currents of one- and two-pion range. *Phys. Rev.*, C78:064002, 2008.

[40] S. Pastore, L. Girlanda, R. Schiavilla, M. Viviani, and R. B. Wiringa. Electromagnetic Currents and Magnetic Moments in (chi)EFT. *Phys. Rev.*, C80:034004, 2009.

[41] S. Pastore, L. Girlanda, R. Schiavilla, and M. Viviani. The two-nucleon electromagnetic charge operator in chiral effective field theory (χEFT) up to one loop. *Phys. Rev.*, C84:024001, 2011.

[42] S. Kolling, E. Epelbaum, H. Krebs, and Ulf-G. Meißner. Two-pion exchange electromagnetic current in chiral effective field theory using the method of unitary transformation. *Phys. Rev.*, C80:045502, 2009.

[43] S. Kolling, E. Epelbaum, H. Krebs, and Ulf-G. Meißner. Two-nucleon electromagnetic current in chiral effective field theory: One-pion exchange and short-range contributions. *Phys. Rev.*, C84:054008, 2011.

[44] H. Krebs, E. Epelbaum, and Ulf-G. Meißner. Nuclear Electromagnetic Currents to Fourth Order in Chiral Effective Field Theory. *Few Body Syst.*, 60(2):31, 2019.

[45] M. Piarulli, L. Girlanda, R. Schiavilla, R. Navarro Pérez, J. E. Amaro, and E. Ruiz Arriola. Minimally nonlocal nucleon-nucleon potentials with chiral two-pion exchange including Δ resonances. *Phys. Rev.*, C91(2):024003, 2015.

[46] Maria Piarulli, Luca Girlanda, Rocco Schiavilla, Alejandro Kievsky, Alessandro Lovato, Laura E. Marcucci, Steven C. Pieper, Michele Viviani, and Robert B. Wiringa. Local chiral potentials with Δ-intermediate states and the structure of light nuclei. *Phys. Rev.*, C94(5):054007, 2016.

[47] M. Piarulli et al. Light-nuclei spectra from chiral dynamics. *Phys. Rev. Lett.*, 120(5):052503, 2018.

[48] A. Baroni et al. Local chiral interactions, the tritium Gamow-Teller matrix element, and the three-nucleon contact term. *Phys. Rev.*, C98(4):044003, 2018.

[49] Maria Piarulli and Ingo Tews. Local Nucleon-Nucleon and Three-Nucleon Interactions Within Chiral Effective Field Theory. *Front. in Phys.*, 7:245, 2020.

[50] Bastian Kubis and Ulf-G. Meißner. Low-energy analysis of the nucleon electromagnetic form-factors. *Nucl. Phys. A*, 679:698–734, 2001.

[51] R. E. Rand, R. F. Frosch, C. E. Littig, and M. R. Yearian. Electron Scattering from the Deuteron at theta=180-degrees. *Phys. Rev. Lett.*, 18:469–472, 1967.

[52] D. Ganichot, B. Grossetete, and D. B. Isabelle. Backward electron-deuteron scattering below 280 mev. *Nucl. Phys. A*, 178:545–562, 1972.

[53] M. Bernheim, E. Jans, J. Mougey, D. Royer, D. Tarnowski, Sylvaine Turck-Chieze, I. Sick, G. P. Capitani, E. De Sanctis, and S. Frullani. DEUTERON ELECTRODISINTEGRATION AT THRESHOLD. *Phys. Rev. Lett.*, 46:402–405, 1981.

[54] S. Auffret et al. EVIDENCE FOR NONNUCLEONIC EFFECTS IN THE THRESHOLD ELECTRODISINTEGRATION OF THE DEUTERON AT HIGH MOMENTUM TRANSFER. *Phys. Rev. Lett.*, 55:1362–1365, 1985.

[55] W. M. Schmitt et al. Deuteron threshold electrodisintegration at high momentum transfer. *Phys. Rev. C*, 56:1687–1699, 1997.

[56] L. E. Marcucci, J. Dohet-Eraly, L. Girlanda, A. Gnech, A. Kievsky, and M. Viviani. The Hyperspherical Harmonics method: a tool for testing and improving nuclear interaction models. *Front. in Phys.*, 8:69, 2020.

[57] J. Carlson, S. Gandolfi, F. Pederiva, Steven C. Pieper, R. Schiavilla, K. E. Schmidt, and R. B. Wiringa. Quantum Monte Carlo methods for nuclear physics. *Rev. Mod. Phys.*, 87:1067, 2015.

[58] A. Amroun et al. H-3 and He-3 electromagnetic form-factors. *Nucl. Phys.*, A579:596–626, 1994.

[59] R. Subedi et al. Probing Cold Dense Nuclear Matter. *Science*, 320:1476–1478, 2008.

[60] J. L. Forest, V. R. Pandharipande, Steven C. Pieper, Robert B. Wiringa, R. Schiavilla, and A. Arriaga. Femtometer toroidal structures in nuclei. *Phys. Rev.*, C54:646–667, 1996.

[61] T. W. Donnelly and I. Sick. ELASTIC MAGNETIC ELECTRON SCATTERING FROM NUCLEI. *Rev. Mod. Phys.*, 56:461–566, 1984.